

FEDSM-ICNMM2010-' \$*) '

MICRO FIBERS MOTION IN A LAMINAR FLOW IN A MICROCHANNEL

Alireza Dastan
Mechanical Engineering Department
Shiraz University
Shiraz, Iran
a.r.dastan@gmail.com

Omid Abouali
Mechanical Engineering Department
Shiraz University
Shiraz, Iran
abouali@shirazu.ac.ir

ABSTRACT

In this paper the motion of micro fibers in a microchannel is studied numerically. The liquid flow regime is considered to be laminar and it is assumed that the fluid and the fibers have a one-way interaction meaning the effects of fibers on the flow are neglected. An inlet plenum of the microchannel with 15 channels considered as the physical domain. The fluid flow in the model is solved numerically by an Eulerian approach using the conventional SIMPLE algorithm. To study the motion of the micro fibers in the flow, the fibers are considered to be ellipsoids of revolution. A code is developed which uses the fluid flow results and solves the equations of ellipsoid motion in a Lagrangian reference frame. The equations of ellipsoid motion consist of three equations for the translational motion and three equations for the rotational motion. The equations are integrated numerically to find the trajectory and the orientation of the micro fibers in the microchannel.

INTRODUCTION

The microchannel heat sink introduced by Tukerman and Pease [1] in the early of 1980's, has become a major consideration area of the researchers in the past two decades. Small mass and volume, large convective heat transfer coefficient, very high surface area to volume ratio and small needed coolant volume are some specific characteristics of microchannels which make them interesting in both research and practical areas. Although, the mentioned advantages make the microchannel unique in the cooling and heat transfer fields, some phenomena affect the main duty of the microchannels as cooling devices. The term "fouling" was originally used in the oil industry and was widely used in the literature to describe any undesirable deposition causing an increase in the thermal resistance of a heat exchanger [2]. Benzinger [3], Yiantsios [4] and Niida [5] have studied the fouling in a microchannel having channels with small hydraulic diameters. Perry and Kandlikar [6] investigated

the fouling in a silicon microchannel with hydraulic diameter of 225 micrometers. They investigated fouling of 4 μm silica and 1.25 μm alumina particles dispersed in water. They observed no particle deposition within the channels because of the high shear stress in flow at the channels compared to the usual channels. It was expressed that there is a secondary effect on the particulate fouling when fibrous elements exist. They observed the fibrous materials with several hundred microns in length caught at the channel entrance. The additional fibers get caught in this fiber web. The fiber web causes an increase in the pressure drop and particle deposition because it acts as a fiber filter. The fibrous material of about 20-microns diameter was found to be from the citric acid buffer solutions used for the preparation of the microfluids. Recently, Dastan and Abouali [7] have studied numerically the effects of fiber web at the channel entrance of a microchannel on the pressure drop and particles collection. It was shown in that study, the fiber web has a considerable effect on the pressure drop in the system and it can act as a fiber filter to collect the particles, as well. So, it is needed to study more about the fibrous element motion and deposition in a microchannel system.

The concept of the fluid with the suspended fibrous particles has many applications in the industry e.g. in composite material production, environment and chemical engineering and paper production industry. The deposition of the inhaled fibrous particles in the respiratory system is important and dangerous for health, as well. So, the investigation of the high aspect ratio particles motion has received the attention of many researchers. Galily and co-workers [8] conducted series of theoretical and experimental study on the motion of ellipsoidal particles. Fan and Ahmadi [9] have studied the effects of shape, aspect ratio and density ratio of particles to fluid on the dispersion of ellipsoidal particles in an isotropic pseudo-turbulent flow field. In addition, they have investigated the deposition of ellipsoidal particles in a turbulent flow [10 and 11]. Chen and Yu [12] and

Högberg et al. [13] have studied the motion of fibers in a laminar flow, as well. Lin et al. [14] have studied the effects of the aspect ratio on the deposition of cylindrical particles by the Lattice-Boltzman method.

In this paper, the motion of fibrous particles in a laminar flow in the inlet plenum of a microchannel is investigated numerically. The fibrous elements are considered to be ellipsoids of revolution. In contrast with spherical particles, the orientation and rotation of particles with high aspect ratio may not be neglected. This makes the solution procedure more complicated in both mathematics and computation. The equations of ellipsoidal particle motion in a given flow field will be explained in the following sections. This study is a first step for the prediction of a fiber web formation at the entrance of the microchannels.

NOMENCLATURE

A	rotation matrix
a	fiber semi minor axis (m)
b	fiber semi major axis (m)
F	force (N)
g	gravity acceleration (m/s^2)
I	moments of inertia($kg.m^2$)
K	resistance matrix
m	mass (kg)
P	pressure (Pa)
T	torque (N.m)
V, u	velocity vector (m/s)
Greek symbols	
β	aspect ratio
μ	dynamic viscosity (kg/m.s)
ρ	density (kg/m^3)
ν	kinematic viscosity (m^2/s)
φ, θ, ψ	Euler angles
ε_i, η	Euler parameters
τ	relaxation time (s)
ω	angular velocity (rad/s)
Superscripts	
fib	Fiber
fld	Fluid
h	hydrodynamic

MODEL DESCRIPTION

An inlet plenum of a microchannel with a circular inlet and 15 fluid carrier channels is considered as the physical domain of the problem. The plenum inlet which is connected to the top of the plenum is a circular duct with the diameter of 1.5 mm. Each fluid carrier channels of the system has a cross section with 205 μm in width and 251 μm in depth. To reduce the size of the computational domain the channel part of the system is not simulated and the entrance of the channels is considered as the outlet of the computational domain. The separating fin between each channel is 97 μm wide. The plenum depth and length are 300 μm and 2.5 mm, respectively.

According to the above explained model, the physical domain has the dimensions of $2500 \times 4433 \times 300 \mu m$. A schematic view of the plenum is shown in figure 1. The origin of the inertial

coordinate system is located at the center of the circular inlet duct at the bottom of the plenum while the Z axis is perpendicular to the bottom wall. The left wall of the plenum (figure 1) is located at $x = -1050 \mu m$ and the entrance of the channels is located at $x = +1450 \mu m$. The inlet plane is located at $z = +300 \mu m$, as well. All properties of the fluid correspond to water at 23C and assumed to be constant. The density and dynamic viscosity of the water in this temperature are $\rho_f = 997.6 \text{ Kg/m}^3$ and $\mu_f = 9.3958 \times 10^{-4} \text{ Kg/m.s}$, respectively. The fiber density is $\rho_o = 2400 \text{ Kg/m}^3$.

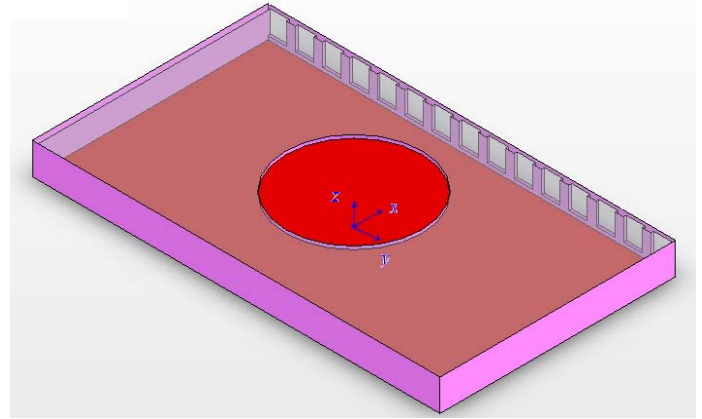


Figure 1. Schematic view of the inlet plenum.

NUMERICAL METHOD

Some simplifications are assumed before solving the governing equations. The steady incompressible flow with constant fluid properties was considered. The flow is laminar. The only body force is the gravitational force which acts in the direction of the plenum depth. Based on these assumptions the fluid governing equations are continuity and momentum as the following:

$$\vec{\nabla} \cdot \vec{V} = 0 \quad (1)$$

$$\vec{\nabla} \cdot \nabla \vec{V} = -\frac{1}{\rho} \vec{\nabla} P + \nu \nabla^2 \vec{V} + \vec{F} \quad (2)$$

The mass flow rate boundary condition is used at the inlet duct. Also, at each channel entrance considered as the outlet of the domain, the mass flow rate of the fluid is set to be 1/15 of total inlet flow rate. No-slip boundary condition is used for all walls. A combination of the structured and unstructured computational grid is used for the grid generation process. An unstructured grid is generated in the area around the circular duct, while a structured grid is used for the other parts of the domain. The whole computational domain cell numbers were found to be a bit more than 1,000,000 cells.

The governing equations (1 and 2) and corresponding boundary conditions are solved by an Eulerian approach. The solution is based on the finite volume method by employing the SIMPLE algorithm. The convective terms are discretized by an upwind scheme and the viscous terms by the central differencing.

For the grid study purpose, a solution-adaptive grid refinement is performed using the curvature approach [15]. The velocity gradient value is calculated for the whole domain and 10% of the maximum gradient value is selected as a refinement threshold. The cells with gradient values more than the threshold are refined. By using a finer grid no noticeable change in numerical results (less than 2%) was observed so the initial computational grid was selected.

Figure 2 shows three coordinate systems used in the motion investigation of ellipsoidal particles, where $\mathbf{x} = [x, y, z]$ is the inertial coordinate system and $\hat{\mathbf{x}} = [\hat{x}, \hat{y}, \hat{z}]$ is the particle coordinate system while its origin is on the mass center of the particle and the \hat{z} axis is along the major axis of the particle. The third coordinate system $\hat{\hat{\mathbf{x}}} = [\hat{\hat{x}}, \hat{\hat{y}}, \hat{\hat{z}}]$ is co-moving frame coordinate system with its origin is located on the origin of particle coordinates and its axes being parallel to the axes of inertial coordinate system.

The transformation from a given Cartesian coordinate system to another can be carried out by means of three successive rotations. The Euler angles (ϕ, θ, ψ) are defined as three successive angles of rotations. The Euler angles used here as the x-convention of Goldstein [16]. Figure 3 shows the definition of the Euler angles.

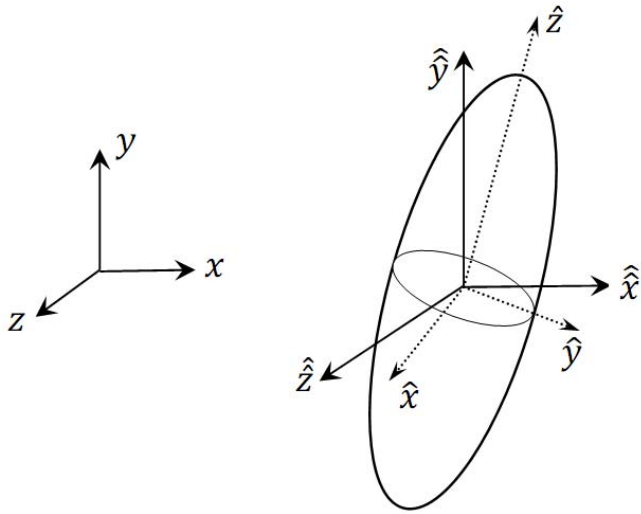


Figure 2. Three different coordinate systems used for the simulation of motion of nonspherical particles.

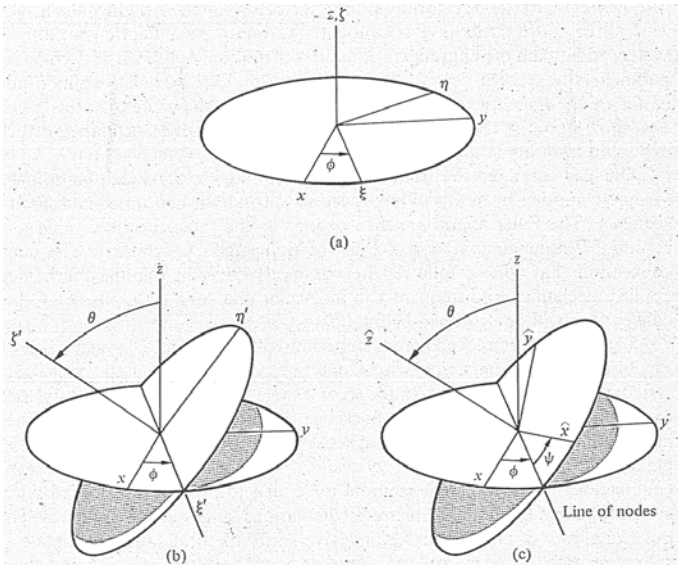


Figure 3. The transformation between two Cartesian coordinate systems through three successive rotations. Euler angles are the angle of rotation in each step. [16]

The transformation between the co-moving frame coordinates and the particle coordinates is given by a linear transformation:

$$\hat{\mathbf{x}} = \mathbf{A}\hat{\hat{\mathbf{x}}} \quad (3)$$

Where A matrix may be expressed as a function of Euler angles [16], i.e.

$$\mathbf{A} = \begin{bmatrix} c\psi c\phi - c\theta s\phi s\psi & c\psi s\phi - c\theta c\phi s\psi & s\psi s\theta \\ -s\psi c\phi - c\theta s\phi c\psi & -s\psi s\phi + c\theta c\phi c\psi & c\psi s\theta \\ s\theta s\phi & -s\theta c\phi & c\theta \end{bmatrix} \quad (4)$$

Where $s\phi = \sin(\phi)$ and $c\phi = \cos(\phi)$.

Due to the singularity in the calculation for the time rates of changes of Euler angles [11], the transformation matrix of A based on the Euler parameters $(\epsilon_1, \epsilon_2, \epsilon_3, \eta)$ is used in the simulation of particle motion, i.e.

$$\mathbf{A} = \begin{bmatrix} 1 - 2(\epsilon_2^2 + \epsilon_3^2) & 2(\epsilon_1\epsilon_2 + \epsilon_3\eta) & 2(\epsilon_1\epsilon_3 - \epsilon_2\eta) \\ 2(\epsilon_2\epsilon_1 - \epsilon_3\eta) & 1 - 2(\epsilon_3^2 + \epsilon_1^2) & 2(\epsilon_2\epsilon_3 + \epsilon_1\eta) \\ 2(\epsilon_3\epsilon_1 + \epsilon_2\eta) & 2(\epsilon_3\epsilon_2 - \epsilon_1\eta) & 1 - 2(\epsilon_1^2 + \epsilon_2^2) \end{bmatrix} \quad (5)$$

Where the Euler parameters are related to Euler angles by [16] :

$$\epsilon_1 = \cos \frac{\phi - \psi}{2} \sin \frac{\theta}{2} \quad \epsilon_2 = \sin \frac{\phi - \psi}{2} \sin \frac{\theta}{2} \quad (6)$$

$$\epsilon_3 = \sin \frac{\phi + \psi}{2} \cos \frac{\theta}{2} \quad \eta = \cos \frac{\phi + \psi}{2} \cos \frac{\theta}{2}$$

The above equations relate a set of four parameters to one of three parameters. Therefore, the Euler's four parameters are subjected to a constraint given by:

$$\epsilon_1^2 + \epsilon_2^2 + \epsilon_3^2 + \eta^2 = 1 \quad (7)$$

The details of derivation of translation and rotation motion equations of ellipsoidal particles have been described in the references [10] or [11]. Therefore, only a summary of the equations is provided here.

Basic equations of translational and rotational motions of a nonspherical particle can be expressed by

$$m^{fib} \frac{d\vec{v}}{dt} = (m^{fib} - m^{fld})\vec{g} + \vec{f}^h \quad (8)$$

$$I_{\hat{x}} \frac{d\omega_{\hat{x}}}{dt} - \omega_{\hat{y}}\omega_{\hat{z}}(I_{\hat{y}} - I_{\hat{z}}) = T_{\hat{x}}^h \quad (9)$$

$$I_{\hat{y}} \frac{d\omega_{\hat{y}}}{dt} - \omega_{\hat{z}}\omega_{\hat{x}}(I_{\hat{z}} - I_{\hat{x}}) = T_{\hat{y}}^h \quad (10)$$

$$I_{\hat{z}} \frac{d\omega_{\hat{z}}}{dt} - \omega_{\hat{x}}\omega_{\hat{y}}(I_{\hat{x}} - I_{\hat{y}}) = T_{\hat{z}}^h \quad (11)$$

Where the translational motion equation is expressed in the inertial coordinate system and the rotational motion equations are expressed in the particle coordinate.

The expression for the hydrodynamic drag force (f^h) acting on an ellipsoidal particle was derived by Brenner [17] as follows:

$$f^h = \mu\pi a\hat{\hat{K}} \cdot (\mathbf{u} - \mathbf{v}) \quad (12)$$

Where a is the semi minor axis of the particle and \vec{u} is the fluid velocity vector at the mass center of particle. The resistance tensor $\hat{\hat{K}}$ is given by

$$\hat{\hat{K}} = \mathbf{A}^{-1}\hat{K}\mathbf{A} \quad (13)$$

Where \hat{K} is a diagonal matrix where:

$$k_{\hat{x}\hat{x}} = k_{\hat{y}\hat{y}} = \frac{16(\beta^2-1)}{\left[\frac{2\beta^2-3}{\sqrt{\beta^2-1}} \ln(\beta+\sqrt{\beta^2-1}) + \beta \right]} \quad (14)$$

$$k_{\hat{z}\hat{z}} = \frac{8(\beta^2-1)}{\left[\frac{2\beta^2-1}{\sqrt{\beta^2-1}} \ln(\beta+\sqrt{\beta^2-1}) + \beta \right]} \quad (15)$$

And β is the particle aspect ratio.

The expression for the hydrodynamic torque (T^h) acting on an ellipsoid was obtained by Jeffery [18], are given as

$$T_{\hat{x}}^h = \frac{16\pi\mu a^3\beta}{3(\beta_o + \beta^2\gamma_o)} [(1 - \beta^2)d_{\hat{z}\hat{y}} + (1 + \beta^2)(w_{\hat{z}\hat{y}} - \omega_{\hat{x}})] \quad (16)$$

$$T_{\hat{y}}^h = \frac{16\pi\mu a^3\beta}{3(\beta^2\gamma_o + \alpha_o)} [(\beta^2 - 1)d_{\hat{x}\hat{z}} + (1 + \beta^2)(w_{\hat{x}\hat{z}} - \omega_{\hat{y}})] \quad (17)$$

$$T_{\hat{z}}^h = \frac{32\pi\mu a^3\beta}{3(\alpha_o + \beta_o)} (w_{\hat{y}\hat{x}} - \omega_{\hat{z}}) \quad (18)$$

Where d_{ij} and w_{ij} are the elements of the deformation rate and spin tensors, respectively.

$$d_{ij} = \frac{1}{2} \left(\frac{\partial u_i}{\partial x_j} + \frac{\partial u_j}{\partial x_i} \right) \quad (19)$$

$$w_{ij} = \frac{1}{2} \left(\frac{\partial u_i}{\partial x_j} - \frac{\partial u_j}{\partial x_i} \right) \quad (20)$$

It should be noted that the velocity gradient in the above equations is in the particle coordinates and it could be obtained by using the following transformation

$$\hat{G} = A \hat{G} A^{-1} \quad (21)$$

The dimensionless parameters α_o , β_o and γ_o in the equations 16-18 are as the following:

$$\alpha_o = \beta_o = \frac{\beta^2}{\beta^2-1} + \frac{\beta}{2(\beta^2-1)^{3/2}} \ln \left(\frac{\beta-\sqrt{\beta^2-1}}{\beta+\sqrt{\beta^2-1}} \right) \quad (22)$$

$$\gamma_o = -\frac{2}{\beta^2-1} - \frac{\beta}{2(\beta^2-1)^{3/2}} \ln \left(\frac{\beta-\sqrt{\beta^2-1}}{\beta+\sqrt{\beta^2-1}} \right) \quad (23)$$

The volume of an ellipsoidal particle is

$$V = \frac{4}{3}\pi a^3\beta \quad (24)$$

and the principal moments of inertia are given by

$$I_{\hat{x}} = I_{\hat{y}} = \frac{(1+\beta^2)a^2}{5} m^{fib} \quad (25)$$

$$I_{\hat{z}} = \frac{2a^2}{5} m^{fib}$$

The time rates of change of Euler parameters are given by

$$\begin{bmatrix} \frac{d\varepsilon_1}{dt} \\ \frac{d\varepsilon_2}{dt} \\ \frac{d\varepsilon_3}{dt} \\ \frac{d\eta}{dt} \end{bmatrix} = \frac{1}{2} \begin{bmatrix} \eta\omega_{\hat{x}} - \varepsilon_3\omega_{\hat{y}} + \varepsilon_3\omega_{\hat{z}} \\ \varepsilon_3\omega_{\hat{x}} + \eta\omega_{\hat{y}} - \varepsilon_1\omega_{\hat{z}} \\ -\varepsilon_2\omega_{\hat{x}} + \varepsilon_1\omega_{\hat{y}} + \eta\omega_{\hat{z}} \\ -\varepsilon_1\omega_{\hat{x}} - \varepsilon_2\omega_{\hat{y}} + \varepsilon_3\omega_{\hat{z}} \end{bmatrix} \quad (26)$$

And the particle position can be easily obtained from

$$\frac{dx}{dt} = \mathbf{v} \quad (27)$$

A computer code was developed to solve the above mentioned equations of ellipsoidal particle motion in a general flow field. For the numerical integration of the equations 8-11 a mixed procedure is used as the one used by Fan and Ahmadi [11]. The time derivations on the left-hand sides are discretized by forward differencing. In each equation, the particle translational or angular velocities on the right hand side corresponding to the dependent variable in the time derivative term is evaluated at the next time step, and all the other terms are evaluated at the current time step. Equations 26 and 27 are discretized by the simple explicit Euler scheme. The integration time step is chosen to be about one order smaller than the ellipsoid particle relaxation time given by:

$$\tau = \frac{2\rho^{fib} g a^2 \beta}{9\mu U} \quad (28)$$

The developed code algorithms follow the next steps:

1- The initial location, orientation, translation and angular velocity of the particle are inputted to the code. The initial orientation of the particle is expressed based on Euler angles, and then they will be transformed to Euler parameters through equation 6.

2- Using equation 5 to calculate matrix A.

3- The fluid velocity and the fluid velocity gradient are estimated at the mass center of the particle due to a Shepard interpolation procedure [19] by choosing data values from the nodes of cell that includes the particle.

4- Equations 8-11, 26 and 27 are solved to find the new particle location and orientation.

5- The solution process returns to step 2 until the particle attaches to the wall or leave the domain (the desired time period of the solution is chosen enough long to ensure that the particle reaches to a boundary).

One of the problems occurred in the particle tracking is to find the computational cell which includes the particle. This process may take many computational and time efforts. The concept of neighbor cells is used to solve this problem. In the beginning of the solution procedure two kinds of neighbors of a cell are determined for each cell by using an auxiliary structured mesh (ASM). The first degree neighbors have a common face with the cell and the second degree neighbors have a common node with it. If the integration time step is chosen properly, the particle leaving the cell has to enter one of the neighbor cells. This concept makes the particle tracking process easy and reduces the computational time.

Because of non-iterative nature of the solution, the computational error grows in time and causes the Euler parameters not to satisfy the equation 7 exactly. To prevent the increase of error, at the end of each time step, the calculated Euler parameters are normalized to ensure us the equation 7 is satisfied.

In the first step of simulation, it is assumed that the particle attaches to the wall when its surface touches the wall. This condition can be achieved for the spherical particles when the center of particle distance to the wall would be smaller than the particle radius. But the situation is more complicated for the ellipsoidal particles. Based on the idea introduced by Fan and Ahmadi [11], a general approach was developed to find the touch point of the ellipsoid to an arbitrary given wall.

When an ellipsoid touches a wall, the touch point is located on the symmetric plane of the ellipsoid perpendicular to the wall. So, in the deposition of an ellipsoid the problem is transformed from a 3-D domain to a 2-D one. This means, it is enough to find the touch point of an ellipse -the intersection of the ellipsoid and the perpendicular plane of the wall- to the wall. Two coordinate systems $\xi\zeta$ and $\hat{\xi}\hat{\zeta}$ are considered at the centre of the ellipse, as shown in figure 4. The ζ axis of $\xi\zeta$ system is normal to the wall and $\hat{\xi}$ axis of $\hat{\xi}\hat{\zeta}$ system is aligned in the direction of particle major axis. The angle between two mentioned coordinate systems, α , can be found using the properties of inner and cross products and the rotation matrix A. By using equation 3, the $\hat{\xi}$ vector with respect to inertial coordinate system is expressed as $\hat{\xi} = [a_{31}, a_{32}, a_{33}]$ where a_{ij} are the elements of rotation matrix of A. A cross product of $\hat{\xi}$ and the normal vector of the wall leads to the normal vector of the ellipse plane and another cross product of this vector and normal vector of the wall leads to the ξ axis which is parallel to the wall. Using the concept of the inner product of vectors ξ and $\hat{\xi}$, the α angle can be found.

According to the detailed discussion carried out in reference [11], the location of touch point in the $\xi\zeta$ coordinate system is given by

$$\xi^* = \frac{\sqrt{(b^2 - a^2)^2 \left[\left(\frac{\cos \alpha}{a} \right)^2 + \left(\frac{\sin \alpha}{b} \right)^2 \right] \sin^2 \alpha \cos^2 \alpha}{\left[1 + a^2 b^2 \left(\frac{1}{a^2} - \frac{1}{b^2} \right) \sin^2 \alpha \cos^2 \alpha \right]} \quad (29)$$

$$\zeta^* = \frac{-\xi^* \left(\frac{1}{a^2} - \frac{1}{b^2} \right) \sin \alpha \cos \alpha - \sqrt{\left(\frac{\cos \alpha}{a} \right)^2 + \left(\frac{\sin \alpha}{b} \right)^2 - (\xi^*/ab)^2}}{\left(\frac{\cos \alpha}{a} \right)^2 + \left(\frac{\sin \alpha}{b} \right)^2} \quad (30)$$

With the equations 29 and 30 and the coordinate of mass center of the particle, the touch point of the ellipsoid to the wall can be determined easily.

RESULTS AND DISCUSSION

The flow field is solved for three different total inlet flow rates of 20.2, 29.4 and 38.6 mL/min. These values are chosen in a way that the average velocity in the channels will be 0.44, 0.64 and 0.84 m/s respectively. Figure 5 shows the velocity contour for the total flow rate of 29.4 mL/min in a horizontal plane located at the middle of channel depth ($z = 175.5 \mu\text{m}$). The maximum velocity in the plane happens at the channel entrance region. The fluid velocity almost vanishes at both left corners of the plenum. To prevent the collection of particles in these two recirculation zones, the microchannels should be designed with round plenum corners.

Figure 6 shows the velocity contour for the total flow rates of 29.4 mL/min at the central vertical plane of the plenums. The inlet fluid is divided into two parts. One flows into the right side and the other flows into left side, making a circulation zone. The stagnation point at the channel plenum bottom wall can be seen easily.

In this paper, it is assumed that the particles have a one-way interaction with the fluids, meaning the effects of the particles on the flow are neglected. The particle motion study is done by a Lagrangian approach.

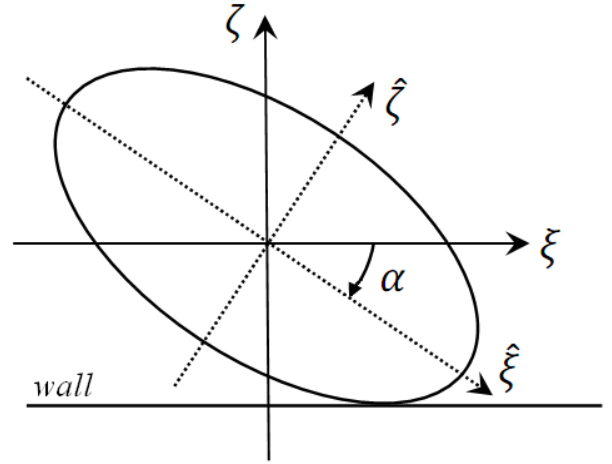


Figure 4. Two coordinate systems are used to find the touch point of an ellipsoid.

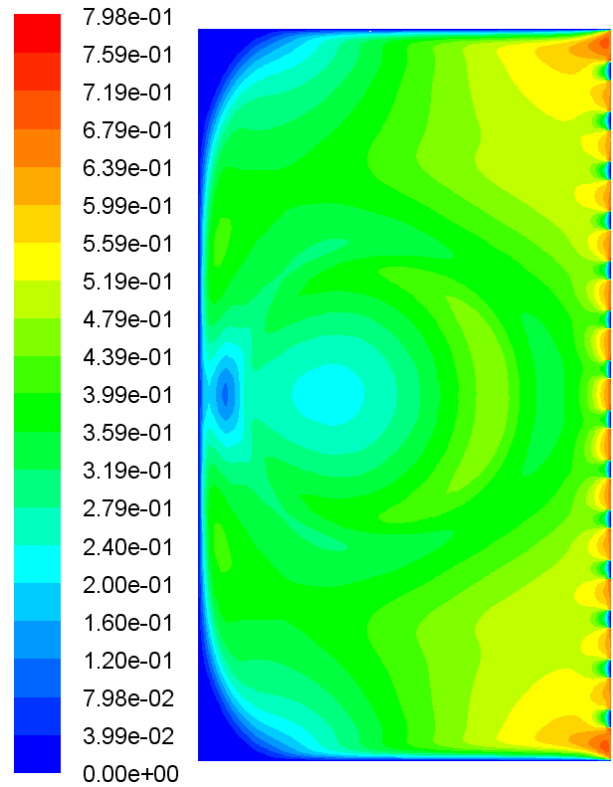


Figure 5. The velocity contours in a horizontal plane at $z=175.5 \mu\text{m}$ in the total flow rate of 29.4 mL/min

To validate the developed code for solving the particle motion equations, a fully developed laminar flow in a pipe is considered. The xz plane of the inertial coordinate system is located at the cross section of the pipe while the y axis is along the pipe length. The average velocity of the fluid is 0.12 m/s while the pipe diameter is 2 mm and the fluid density and dynamic viscosity are assumed to be $\rho_f=1 \text{ Kg/m}^3$ and $\mu_f=1 \times 10^{-5} \text{ Kg/m.s}$, respectively. An ellipsoidal particle with semi minor axis of $a = 5 \mu\text{m}$, aspect ratio of $\beta=20$ and density of $\rho_p=1000 \text{ Kg/m}^3$ is injected in the flow. The initial location of the particle

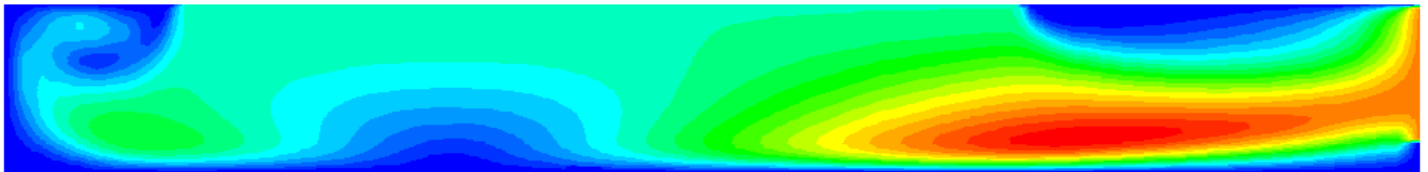


Figure 6. The velocity contours in a vertical plane at $y=0$ in the total flow rate of 29.4 mL/min (the color values are the same as those of figure 5)

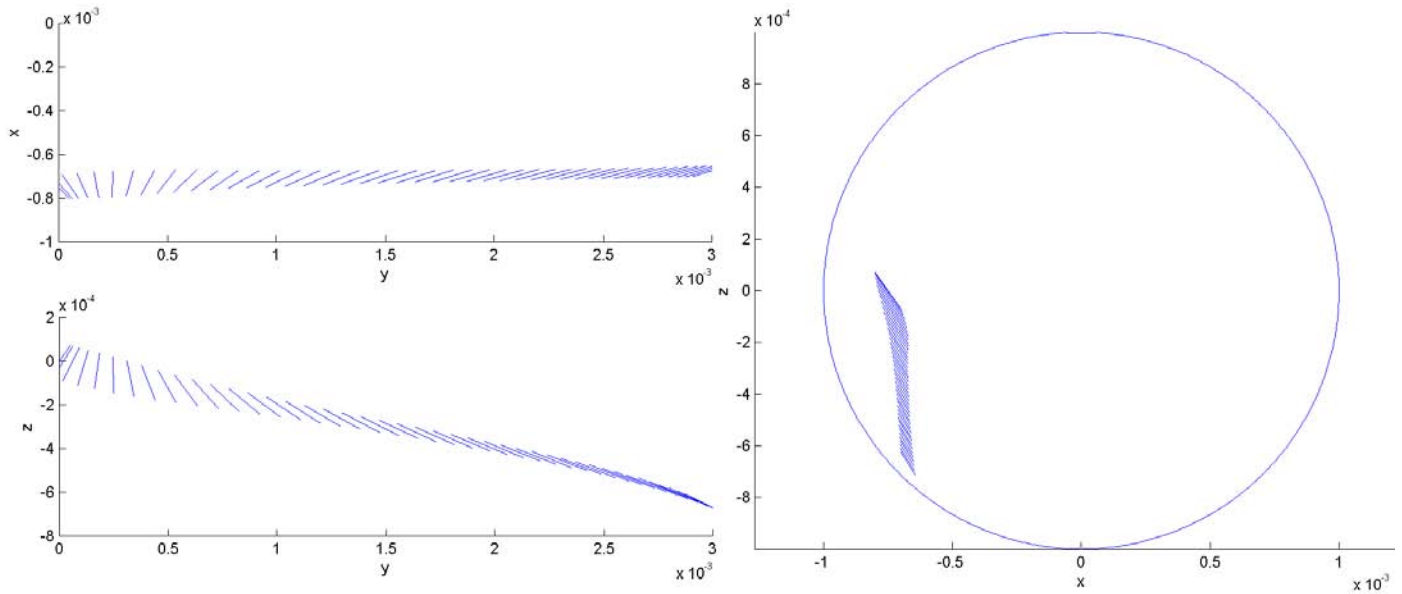


Figure 7. The trajectory of a fiber in a fully developed pipe flow in three different planes.

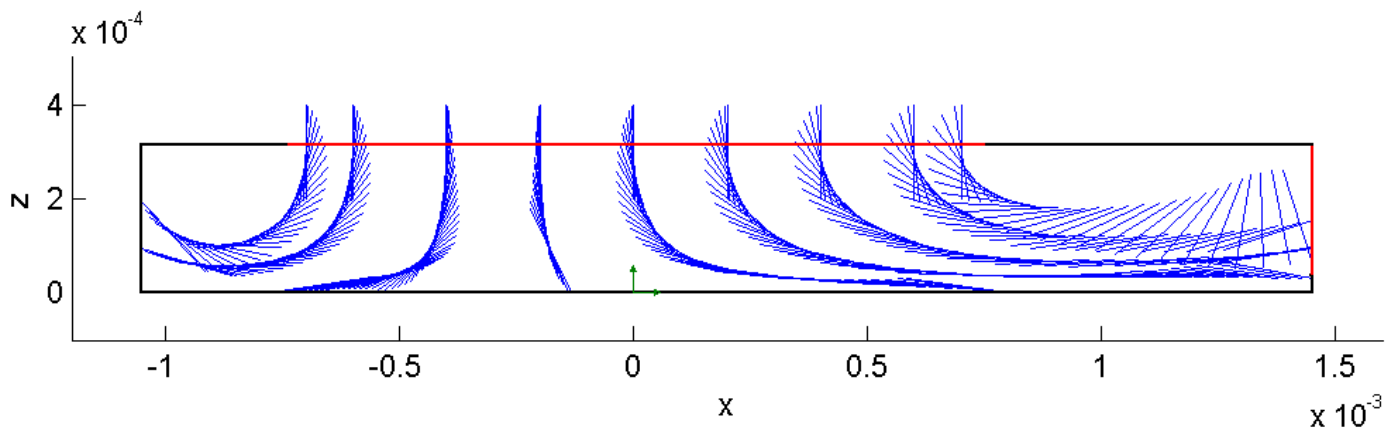


Figure 8. The trajectories of the similar fibers which injected in different locations at the central plane of the plenum.

is set as $x_0=0.75 R$ (R is the pipe radius) and $z_0=0$. The initial Euler angles are $\phi_0=45^\circ$, $\theta_0=-45^\circ$ and $\psi_0=0^\circ$. The particle relaxation time based on the equation 28 is $\tau = 0.905$. Figure 7 shows the location and orientation of the fiber in three different planes. The results are in a very good agreement with those offered by Chen and Yu [12] and Högberg [13]. In the pipe flow, the fiber rotates because of the hydrodynamic torque and tends to align with the flow while moving in the streamwise direction. The small drift motion is also observed in the x -direction.

Figure 8 shows the trajectories of the injected ellipsoids in the total flow rates of 20.2 mL/min in the studied microchannel plenum. The semi minor axis of the ellipsoid and the aspect ratio are 10 μm and 10, respectively. The particles injected at the central plane of the plenum at the duct inlet having different x -coordinate locations ($y=0$, $z=300 \mu\text{m}$). The particle orientation is in a way that the fiber major axis aligns in the z direction, so three initial Euler angles is set to be zero. The particle does not tend to move in the y -direction, because the velocity gradient vanishes at the central plane of the plenum. So, the motion of the particle in the y -direction is not shown. The major axis of the injected particles is assumed to be in the direction of inlet fluid. Therefore the initial Euler angles vanish. The results show that the mass center of the fiber almost follows the flow path line passes through the injection point of the fiber as the spherical particles [7]. The orientation of the fiber in the flow is a direct function of the velocity gradient. The rotation direction of the fiber follows a simple qualitative rule. Considering the direction of the translational motion of the fiber, it rotates in a way that the fiber passes from high velocity region to the lower velocity one in a direction consistent with the streamwise. For instance, as shown in the figure, both particles injected from $x=200 \mu\text{m}$ and $x=700 \mu\text{m}$ move in the right hand side direction. According to figure 6, the high velocity region is between the paths of these two particles. For the lower particle (injected at $x=200 \mu\text{m}$), the high velocity region is at the above of the particle location and therefore the particle rotates clock wise. On the other hand, for the upper one (injected at $x=700 \mu\text{m}$), the particle rotates counter clock wise. In summary, the rotation of the fiber in a given flow field is a complicated phenomenon which is a function of the velocity gradient (rate of shear) and the particle motion direction. Furthermore, the complicated behavior of the flow field in the microchannel geometry makes the prediction of the fiber orientation difficult.

The trajectories of three similar fibers injected at $x=400 \mu\text{m}$ in three different flow rates are shown in figure 9. As shown in the figure, the trends of motion of the fibers in all three cases are similar but only the z -coordinate of the fibers is different. It may be because of the increase of the z -direction velocity of the fluid which causes the particle to be transferred to the lower z -coordinate before it changes its motion direction to the outlet boundary.

To study the effects of the aspect ratio of the fibers on their motion, 5 different fibers with the same volume and different aspect ratio are considered. They were injected to the flow with the flow rate of 38.6 mL/min from the same location. The trajectories of the particles are shown in figure 10. The particles with smaller aspect ratio tend to move in the lower location in z

direction, near the bottom wall of the plenum, where the shear rate is high relatively. The higher velocity gradient which the fiber experiences in the near wall motion makes the behavior of the particle different. Two fibers with lower aspect ratios ($\beta=3$ and $\beta=5$) rotate counter clock wise and touch the wall before they can leave the domain as the other particles.

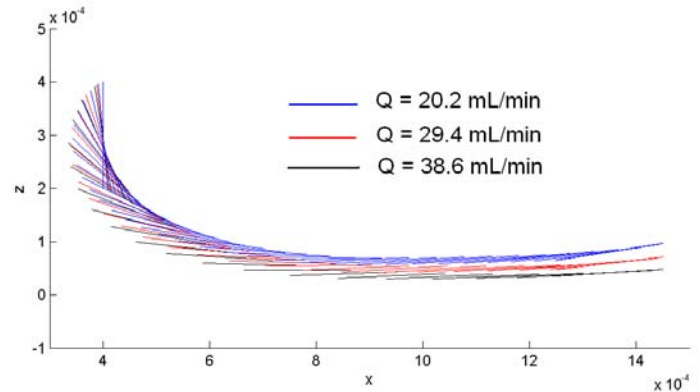


Figure 9. The trajectories of three similar fibers at different total flow rates of the fluid.

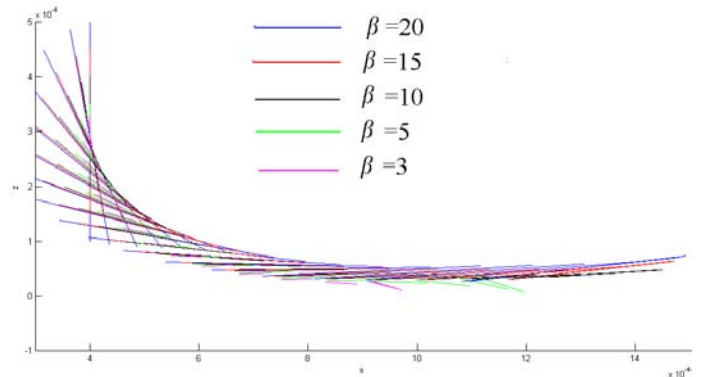


Figure 10. The trajectories of the fibers with the same volume and different aspect ratio for the flow rate of 38.6 mL/min

CONCLUSION

In this paper the flow field in a plenum of a microchannel with 15 channels and one circular inlet duct was solved numerically in three different flow rates. A general code which solves the equations of an ellipsoid in a general 3-D flow field was developed. The fiber motion simulation was done by a Lagrangian approach, while the flow field equations were solved by an Eulerian one. The trajectory of a fiber simulated by the code was validated by the results of earlier researchers. It was found that the fiber mass centers follow the path lines which pass through the injection point of the fibers. The orientation of the fibers in the flow is a complicated phenomenon which may not predict without solving the equation of motion. The velocity gradient, aspect ratio and the flow direction are the affecting factors which may change the orientation of the fibers in the flow.

REFERENCES

- [1] Tuckerman, D.B. and Pease, R.F.W., High-performance heat sinking for VLSI, *IEEE Electron. Dev. Lett.*, EDL-2, pp. 126–129, 1981.
- [2] Liu, R., A study of fouling in a heat exchanger with an application of electronic anti-fouling technology, PhD. thesis, Drexel University, Philadelphia, PA, 1999.
- [3] Benzinger, U. et al., Anti fouling investigations with ultrasound in a microstructured heat exchanger, *Proceedings of the 6th International Conference on Heat Exchanger Fouling and Cleaning Challenges and Opportunities*, Kloster Irsee, Germany, 2005.
- [4] Yiantsios, S.G., and Karabelas, A.J., Deposition of micron-sized particles on flat surfaces: effects of hydrodynamic and physicochemical conditions on particle attachment efficiency, *Chemical Engineering Science*, vol. 58, pp. 3105-3113, 2003.
- [5] Niida, T., et al., Removal of adhering particles of polystyrene latex and iron oxide on a wall by shear flow in water, *Particle and Particle. Syst. Charact.*, vol. 6, pp. 69-73, 1989.
- [6] Perry, J. and Kandlikar, S., Investigation of fouling and its mitigation in silicon microchannel, *Proceedings of Sixth International Conference on Nanochannels, Microchannels and Minichannels*, Darmstadt, Germany, ICNMM2008-62038, 2008.
- [7] Dastan, A. and Abouali, O., Numerical investigation of fiber web effects on the pressure drop and particles collection in a microchannel, *Proceedings of seventh International Conference on Nanochannels, Microchannels and Minichannels*, Pohang, South Korea, ICNMM2009-82245, 2009.
- [8] Gallily, I., and Cohen, A., On the Orderly Nature of the Motion of Nonspherical Aerosol Particles: II. Inertial Collision between a Spherical Large Droplet and an Axially Symmetrical Elongated Particle, *J. Colloid Int. Sci.* 68:338-356, 1979.
- [9] Fan, F.-G. and Ahmadi, G., Dispersion of ellipsoidal particles in an isotropic pseudo-turbulent flow field, *J. Fluids Engineering*, Vol. 117, pp. 154-161, 1995.
- [10] Fan, F.-G. and Ahmadi, G., "Wall deposition of small ellipsoids from turbulent air flows: a Brownian dynamics simulation". *Journal of Aerosol Science*, Vol. 31(10), pp. 1205-1229, 2000.
- [11] Fan, F.-G. and Ahmadi, G., A sublayer model for wall deposition of ellipsoidal particles in turbulent streams. *J. Aerosol Sci.* Vol. 26, pp. 831-840, 1995.
- [12] Chen, Y. K. and Yu, C. P., "Sedimentation of Fibers from Laminar Flows in a Horizontal Circular Duct". *Aerosol Science and Technology*, Vol. 14(3), pp. 343 – 347, 1991.
- [13] Högberg, S.M, et al., Numerical model for fiber transport in the respiratory airways, proceeding of The 19th International Symposium on Transport Phenomena, Reykjavik, Iceland, 2008
- [15] Warren, G. P., et al., Grid convergence for adaptive methods. Technical Report AIAA-91-1592, American Institute of Aeronautics and Astronautics, AIAA 10th Computational Fluid Dynamics Conference, Honolulu, Hawaii, 1991.
- [16] Goldstein, H., *Classical Mechanics*, 2nd Edition. Addison-Wesley, Reading, MA, 1980.
- [17] Brenner. H. , The stokes resistance of an arbitrary particles-IV. Arbitrary field of flow. *Chem. Eng. Sci.* Vol. 19, pp. 703-727, 1964.
- [18] Jeffery, G. B. , The motion of ellipsoidal particles immersed in a viscous fluid. *Proc. Roy. Soc. A* 102, 161-179, 1922.
- [19] Press, W.S. et al., *Numerical recipes: the art of scientific computation*, third edition, Cambridge University Press, 2007.